AIP Applied Physics Letters

In-situ observation of self-regulated switching behavior in WO3-x based resistive switching devices

D. S. Hong, W. X. Wang, Y. S. Chen, J. R. Sun, and B. G. Shen

Citation: Applied Physics Letters **105**, 113504 (2014); doi: 10.1063/1.4895629
View online: http://dx.doi.org/10.1063/1.4895629
View Table of Contents: http://scitation.aip.org/content/aip/journal/apl/105/11?ver=pdfcov
Published by the AIP Publishing

In-situ observation of self-regulated switching behavior in WO_{3-x} based resistive switching devices

D. S. Hong, W. X. Wang, Y. S. Chen,[a)] J. R. Sun, and B. G. Shen
Beijing National Laboratory for Condensed Matter Physics and Institute of Physics, Chinese Academic of Sciences, Beijing 100190, China

(Received 3 July 2014; accepted 1 September 2014; published online 15 September 2014)

The transmittance of tungsten oxides can be adjusted by oxygen vacancy (V_o) concentration due to its electrochromic property. Here, we report an *in-situ* observation of resistive switching phenomenon in the oxygen-deficient WO_{3-x} planar devices. Besides directly identifying the formation/rupture of dark-colored conductive filaments in oxide layer, the stripe-like WO_{3-x} device demonstrated self-regulated switching behavior during the endurance testing, resulting in highly consistent switching parameters after a stabilizing process. For very high V_os mobility was demonstrated in the WO_{3-x} film by the pulse experiment, we suggested that the electric-field-induced homogeneous migration of V_os was the physical origin for such unique switching characteristics. [http://dx.doi.org/10.1063/1.4895629]

Because of the physical limit of current Flash memory, researchers have made great efforts to develop the next generation non-volatile memory in recent years. Among many candidates, the resistive random access memory (RRAM), which is based on resistive switching (RS) effect of dielectric material, is considered as the most promising technology due to its simple structure, high speed, good scalability, and low power consumption.[1–3] The RS effect is widely observed in most oxide materials, including NiO,[4,5] TiO_2,[6,7] ZnO,[8,9] HfO_2,[10,11] Ta_2O_5,[12,13] ZrO_2,[14,15] and so on. Previous works indicated that, in most cases, the reversible switching states of RRAM devices were caused by the connection and rupture of conductive filaments (CF) in the insulative layers.[16,17] The CFs could be formed by either metal ions (such as Ag^+, Cu^+) or oxygen vacancies (V_o) in various RS systems.[5,16,17] However, a common problem of the CF based devices is that the shape and location of CF are usually uncontrollable due to the random nature of electric breakdown, which badly affects the uniformity and reliability performance in practical application. To solve this problem, many optimization methods were already proposed, such as the impurity doping,[11] process annealing,[18] active electrode,[19] and nanocrystal inducing.[20–22] By reducing the active energy of ion migration or localizing the driving electric field, the switching characteristics of these devices were significantly improved.

Tungsten oxide is an appropriate RRAM candidate for the high degree of compatibility with conventional complementary metal-oxide semiconductor (CMOS) technique. Stoichiometric WO_3 is a transparent insulator in visible light range for its wide band gap of 2.6 eV. Its optical characteristic can be adjusted by the insertion/extraction of cations or V_os that is known as the electrochromic effect.[23] The appearance of W^{5+}/W^{4+} ions in oxygen-deficient WO_{3-x} phase would both reduce its transmittance as well as resistance.[24] Therefore, when integrating WO_{3-x} film in RRAM devices, it is possible the electric-field-induced resistance transition will also cause distinct transmittance contrast of the local switching region, which gives us an opportunity for the *in-situ* observation of RS dynamics. Moreover, it was reported that the active energy of oxygen ions' (O^{2-}) migration would be significantly lowered by the V_o defects nearby.[25] We wonder what unique characteristics will be found if the O^{2-}s are easily moved in the switched films. In principle, the O^{2-}s with very high ion mobility are inclined to migrate homogeneously in the whole film under applied electric field, which is expected to be more stable and smooth comparing with the random breakdown of a confined region in other RS materials, such as high-κ dielectric HfO_2. In this paper, we systematically investigated the RS characteristics of strip-like Au/WO_{3-x}/Au planar devices. Combining electric measurements and *in-situ* observation, the self-regulated RS behavior and the aspect ratio effect were clearly demonstrated. The high mobility of O^{2-} ions in the WO_{3-x} film were confirmed by the pulse experiment. These unique characteristics present an intuitive and fundamental approach for the device design based on such material.

For device fabrication, 400 nm thick WO_{3-x} film ($x \sim 0.1$) was grown on glass substrate by pulsed laser deposition at 400 °C in 10 Pa oxygen pressure and patterned to 50 μm stripes by lithography technique. Then, 50 nm thick Au electrodes were deposited on the WO_{3-x} stripes by DC sputtering and lift off method. Schematic view of the Au/WO_{3-x}/Au structure is shown in Fig. 1(a). For convenience, the two electrodes were defined as upper electrode (UE) and lower electrode (LE). Three types of devices were prepared for the present experiments with various UE-LE lengths of 100 μm, 50 μm, and 20 μm, respectively. In DC sweep mode, current-voltage (IV) characteristics were measured by a Keithley 2601 source meter. Voltage bias was applied on the UE, and the LE was grounded. During the RS process, the planar device was illuminated by white light from the back side and the transparency of WO_{3-x} film was *in-situ* monitored by a CMOS camera. The surface morphology and conductivity property of the switched film were analyzed by a scanning probe microscopy (SII SPI3800N). In pulse measurements, voltage bias was applied by an Agilent pulse

[a)]E-mail: yschen@aphy.iphy.ac.cn

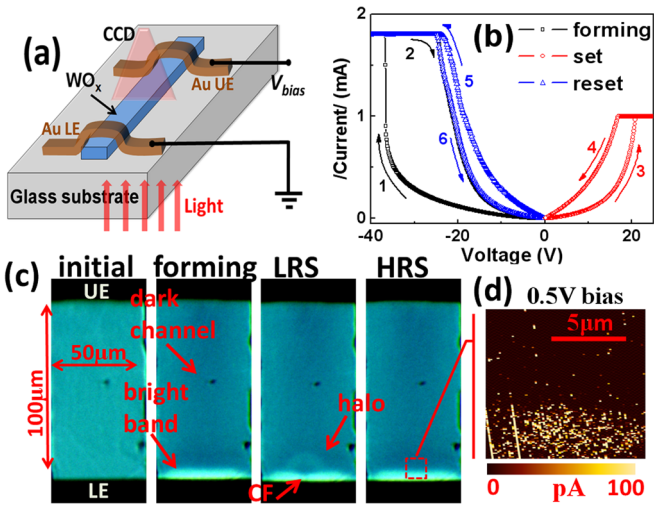

FIG. 1. (a) Schematic view of the planar WO_{3-x} device. (b) IV characteristics of forming, set, and reset processes. Numbers indicate the voltage-sweep sequence. (c) Optical images of initial, forming, LRS, and HRS states of the WO_{3-x} film. (d) A current mapping under 0.5 V bias of the dark/bright interface marked as the dashed square in HRS image, demonstrating obvious conductivity contrast between two regions. The scanning bias of +0.5 V was applied on the UE, and the Rh-coated probe was grounded.

function arbitrary generator 81150 A, and corresponding transient current was captured by a two channel oscilloscope as mentioned previously (Tektronix TDS 3052C).[26]

Figure 1(b) shows the IV characteristic of a Au/WO_{3-x}/Au planar device with the dimensions of 100 μm in length and 50 μm in width. A forming process under negative electric filed first switched the initial device to a high resistance state (HRS). After that, typical bipolar RS behavior was observed: The positive bias set the HRS to a low resistance state (LRS) and then the LRS would be reset back to HRS in the negative direction. Interestingly, using the *in-situ* optical system, a synchronous change in local transmittance of the WO_{3-x} film was observed during the RS process. As shown in Fig. 1(c), the as-deposited film exhibited unified deep blue color. Corresponding to the abrupt current jumping in forming process, a dark-colored channel emerged at the UE and quickly extended to LE side. Simultaneously, a bright band occurred at the LE which prevented the dark channel directly connecting to LE. In the following set process, a fine dark-colored CF was formed in the bright band abruptly, accompanied by the appearance of an annular halo around CF's tip. At last, the CF and the halo would both vanish in the reset process under negative bias. A conductive atomic force microscopy (C-AFM) was used to analyze the local conductivity of different colored regions in the switched WO_{3-x} film. A current mapping of the interface area as marked in the HRS image is shown in Fig. 1(d), which demonstrates the distinct conductivity contrast between dark and bright regions. Generally, the transmittance of WO_{3-x} film would decrease with increased x factor, which represented for the density of W^{5+} ions.[23,24] We thus consider that the coloration of local region in WO_{3-x} film and the co-switching of resistance are both caused by the redistribution of O^{2-}s under external field.[27] When applying negative forming voltage, O^{2-}s in pristine WO_{3-x} film (slightly oxygen-deficient) will move towards the LE side, leading to a more oxygen-deficient channel at the UE with lower transmittance and resistance. Correspondingly, the accumulation of migrated O^{2-}s at LE will form a stoichiometric WO_3 band that is nearly transparent. During the RS cycles, the dark channel acts as a virtual electrode and applied voltage bias mostly drops on the insulative bright band. Naturally, the reproducible appearance/vanishment of the fine CF in the bright band dominates the changes in resistance of LRS/HRS. In addition, the co-appearance of annular halo in the virtual electrode can be understood by the conservation of O^{2-} amount in whole device.

In-situ observation of planar structured device gives us an opportunity to investigate the evolution process of the CF and nearby region. What we want to emphasize here is the strip-like WO_{3-x} devices possess the self-regulated RS behavior during endurance testing. As shown in Fig. 2(a), the set/reset IV curves demonstrate obvious shift in the first few cycles and then tend to be stable after about 20 cycles. The resistance distribution of HRS/LRS in Fig. 2(b) also confirms this variation tendency. The initial HRS of 0.4 MΩ quickly rises with the cycle number and ultimately kept at 0.8 MΩ in average, resulting in a fixed switching window of 25 times. An intuitive feature of the self-regulated behavior was revealed by the LRS images captured after each cycle (Fig. 2(c)). At first, the bright region with an arc shape did not cover the whole LE, leaving the bypass current under applied field. This bright region would laterally spread out in the following RS cycles. And finally, a rectangle-shaped bright band was formed after 20 cycles, which completely separated the dark channel and the LE. The regular shape of blocking band should bring on a uniform distribution of electric field, which may be the origin for the stabilized RS characteristic. The self-regulated behavior is a common phenomenon of our WO_{3-x} devices. Figure 2(d) shows the HRS/LRS distributions of four devices with the same 100 μm length and 50 μm width. We can see that the device-to-device fluctuation is almost overlapped with the cycle-to-cycle fluctuation of a single device. It possibly means, though irregular dark and bright regions are formed in various devices, the self-regulated behavior will always modify each switched layer to the same rectangle shape just after several switching cycles. Above results indicate that the stable switching parameters of WO_{3-x} devices are mainly determined by its intrinsic properties in prior to the random forming process, which shows a feasible way to solve the uniformity and stability problems of RRAM.

Next, we studied the aspect ratio effect of the stripe-like WO_{3-x} devices. Figures 3(a) and 3(b) show the HRS/LRS distributions of other two types of device with UE-LE lengths of 50 μm and 20 μm, respectively. When the stripe length was shorted, we found the stabilizing process of self-regulated behavior became much slower. The 50 μm device needed about 120 cycles to reach its stable state, and the 20 μm device needed more than 400 cycles. Otherwise, the fluctuations of the final HRS/LRS states were larger than that of the 100 μm devices. This difference was correspondingly reflected by the *in-situ* images shown in Fig. 3(c). The bright region still experienced an expansion during the endurance testing, from partially covering to entirely covering the LE. However, the expansion processes of 50 μm and 20 μm devices were no longer limited in the lateral direction but also in

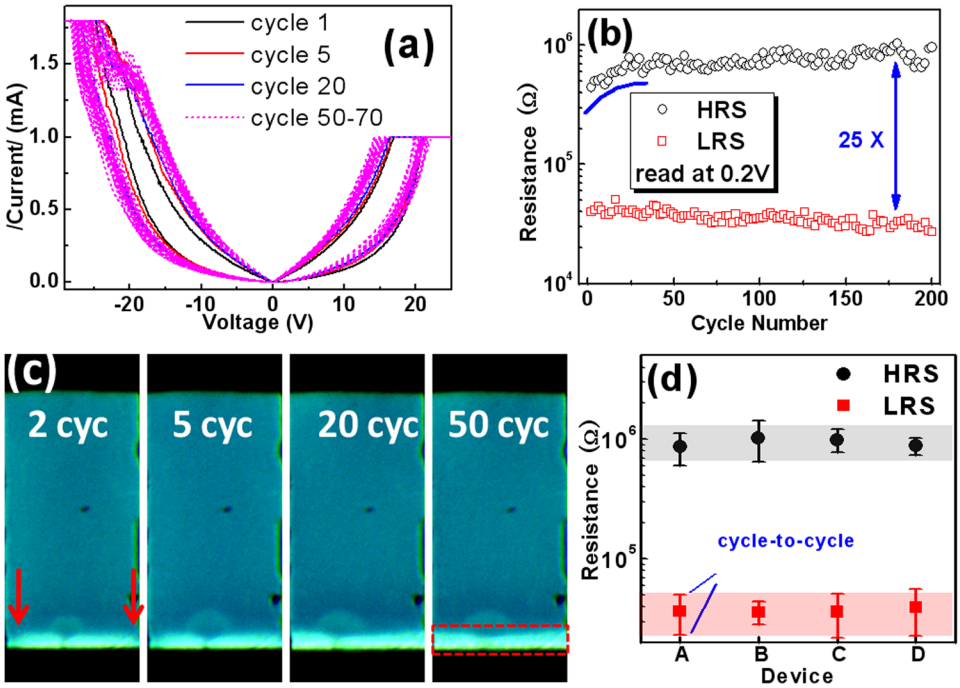

FIG. 2. (a) IV curves of cycle 1, cycle 5, cycle 20, and cycle 50–70 selected from endurance testing of a 100 μm device. (b) HRS/LRS distribution versus cycle number. The read voltage is 0.2 V. (c) Optical images of the LRS captured after different cycle numbers. The arc-like bright band became regular rectangle shape after 20 cycles. (d) Statistical HRS and LRS of four 100 μm device. The error bars represent the cycle-to-cycle fluctuation and the semitransparent bands represent the device-to-device fluctuation.

the vertical direction. As a result, the final bright bands of such devices were not as regular as that of 100 μm device after the stabilizing process.

To further understand above results, electric field distributions of these devices were simulated by the finite element analysis using the parameters extracted from experiment data (Fig. 3(d)). Although the applied voltage mostly dropped on the insulative bright band, highly concentrated electric field intensity still existed in edge area outside the bright band, which was sufficient to drive nearby V_os. As a result, this field leakage will gradually modify the boundary of the special electric structure during repeated switching operations, which is the origin of self-regulated RS behavior. We can see that the field leakage of 100 μm device is mainly along the lateral direction and rectangle-shaped blocking layer is finally formed. By contrast, the field leakage of 20 μm device is along both lateral and vertical direction, which causes the irregular shape of the stabilized bright band shown in Fig. 3(c). The simulation result indicates a larger length/width ratio will be more beneficial to the self-regulated behavior. Moreover, we believe these unique characteristics of WO_{3-x} planar film are also adequate for the vertical device if the electrode size is comparable to film thickness. The homogeneous migration of O^{2-}s following

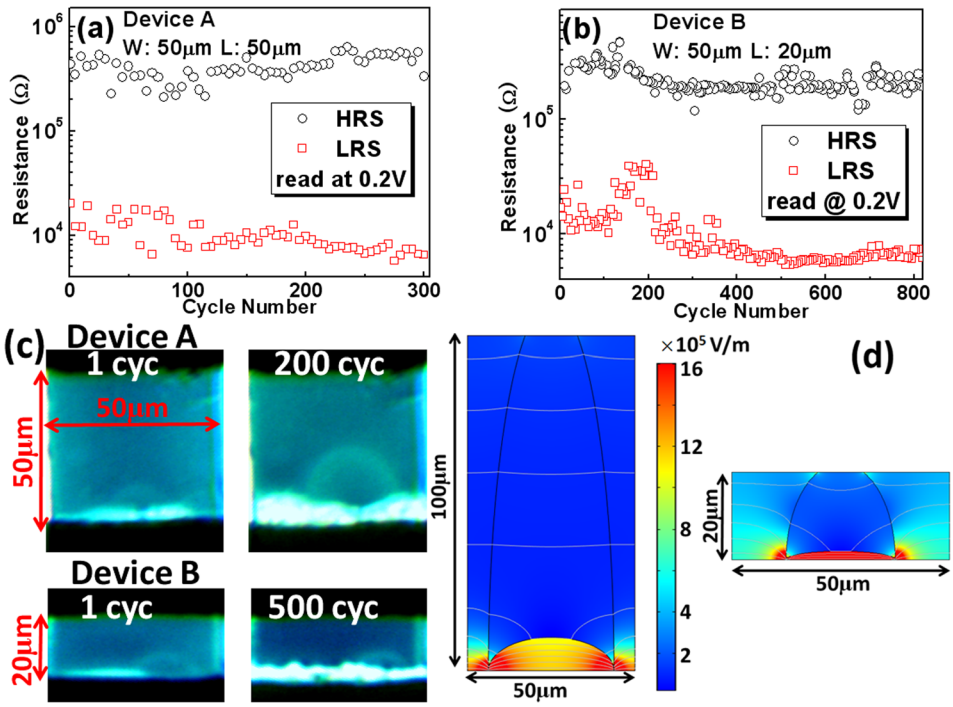

FIG. 3. HRS/LRS distributions versus cycle number for (a) device A with 50 μm length and (b) device B with 20 μm length. The width of WO_{3-x} stripe is 50 μm. (c) LRS images of device A and B. Irregular shapes of bright band occurred after 200 cycles for device A and 500 cycles for device B. (d) Simulations of electric field distribution for the 100 μm and 20 μm devices. The leakage field intensity at the edge of bright band is related to the aspect ratio of WO_{3-x} stripe.

electric field distribution in the bar-like vertical device will significantly suppress the randomicity of RS, which is usually induced by the pre-forming process in different devices.

Sine we considered the O^{2-}s in WO_{3-x} phase were easily distributed along the electric field direction, an experiment was designed to directly measure the ion mobility of O^{2-}. The annular halo in virtual electrode, which was formed by the extra O^{2-}s released from the CF part, could be used as a clear sign for the migration of O^{2-}. As shown in Fig. 4(a), when we applied a series of positive voltage pulses on the LRS, the annular halo would be smoothly enlarged. Vertical line profiles of film transmittance just across the CF's location were extracted from the optical images step by step. Hence, the displacements of the halo (Δx) moving to the UE are directly calculated by the slight peak shifts shown in Fig. 4(b). Changing the pulses' amplitude (20 V, 19 V, and 18 V) and width (1 s, 2 s and 4 s), we got a series of Δx-t (t is the total bias time) data (Fig. 4(c)). The linear slopes of three curves, which represent for the drift velocity v, are 0.6 μms^{-1} for 20 V bias, 0.43μms^{-1} for 19 V bias, and 0.17μms^{-1} for 18 V bias. A simple relation between ion mobility μ and drift velocity is $\mu = v/E_{eff}$, where effective electric intensity E_{eff} is simulated by the finite element analysis. Thus, the deduced μ are $3.5*10^{-9}$ cm^{2}V^{-1}s^{-1} for 20 V bias, 2.1×10^{-9} cm^{2}V^{-1}s^{-1} for 19 V bias and 7.8×10^{-10} cm^{2}V^{-1}s^{-1} for 18 V bias, respectively. The ion mobility of O^{2-} increased with pulse amplitude possibly indicates the effective temperature of the halo region has been modulated by Joule heating effect. We have measured the temperature dependence of IV behavior for the same LRS shown in Figure 4(d). The LRS resistance still demonstrates well semiconducting transport behavior given by[28]

$$\rho_T = \rho_0 \cdot e^{\left(\frac{E_a}{k_B \cdot T}\right)},$$

where ρ_0 is a constant and the active energy of carrier E_a is 0.15 eV given by the fitting data. As shown in Fig. 4(e), when voltage pulses increased from 18 V, 19 V, to 20 V, the steady-values of the LRS resistance would correspondingly decrease from 20 kΩ, 15 kΩ, to 12 kΩ, which meant the effective temperature of the halo was risen up by the enhanced Joule heating effect. Thus, the μ-V_{pulse} relation shown in Fig. 4(f) can be simply explained by the common temperature dependence of ion mobility obeying the following equation:[29]

$$\mu_T = \frac{\mu_0}{T} \cdot e^{\left(-\frac{E_a}{k_B \cdot T}\right)},$$

where E_a is the active energy of O^{2-} ions. In spite of the temperature effect, we considered that such high ion mobility of O^{2-}s is the fundamental reason for the homogeneous switching characteristics in WO_{3-x} based devices.

In summary, simultaneous switching of local transmittance, oxygen content, and resistance state of the planar Au/WO_{3-x}/Au devices were demonstrated by electric measurements combined with *in-situ* optical observation. We found the strip-like WO_{3-x} device possessed self-regulated RS behavior, of which the switching parameters would be stabilized during an endurance testing. The high mobility of O^{2-} ions in WO_{3-x} film measured by pulse experiment was larger than 10^{-9} cm^{2}V^{-1}s^{-1}. We suggested that the homogeneous migration of O^{2-}s along electric field distribution was the physical origin for the self-regulated behavior and aspect ratio effect. The unique RS characteristics of planar WO_{3-x}

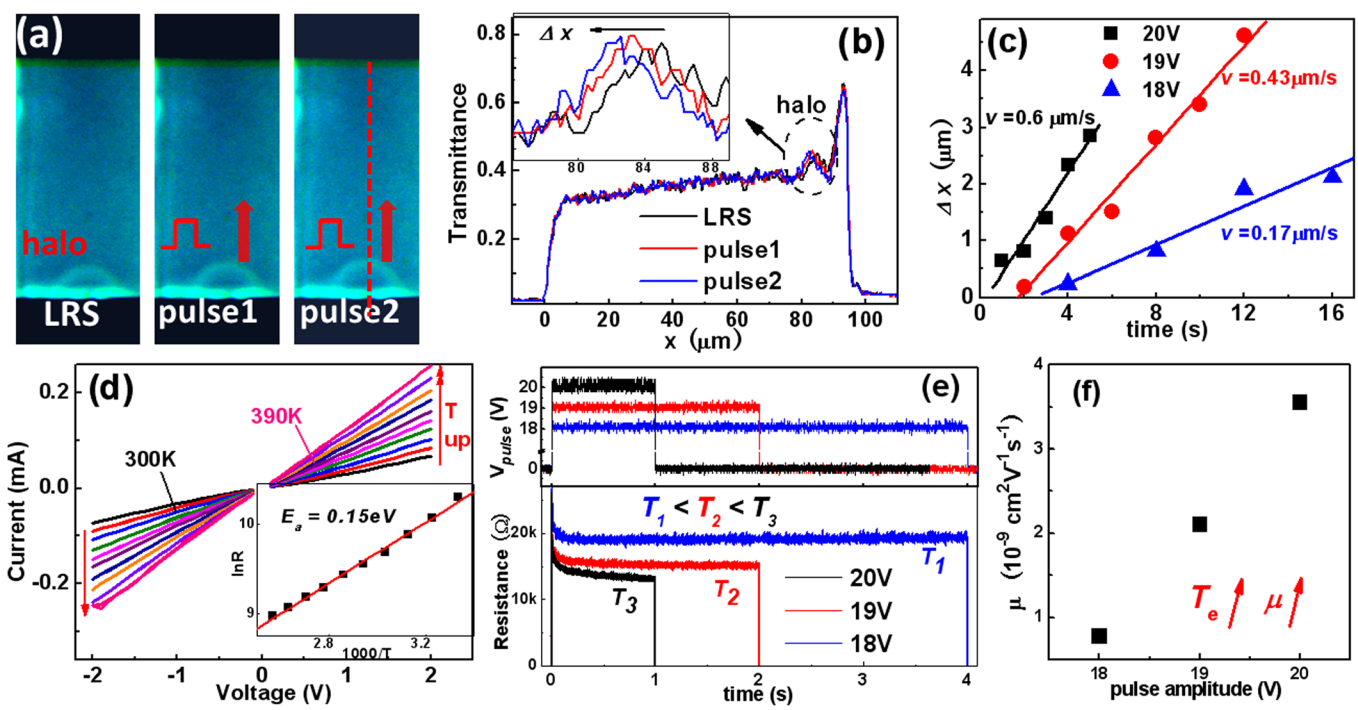

FIG. 4. (a) The annular halo of LRS gradually extended to UE under positive pulses. (b) Line profiles of transmittance across the location of fine CF. Peak shifts of annular halo are shown in the inset enlargment. (c)Δx-t curves under 20 V, 19 V, and 18 V pulses. The slopes represent drift velocity v. (d) IV curves of LRS measured at different ambient temperatures. Inset is a fitting of lnR-1000/T according to semiconducting transport model. (e) Transient responses of the decreasing LRS caused by Joule heating effect under different pulse amplitudes. (f) The u-V_{pulse} relation indicates that the O^{2-} ion mobility is increased with the effective temperature.

stripes give us some fundamental guidance of optimal design for the vertical RRAM devices based on such high ion mobility materials.

This work has been supported by the National Basic Research of China (Nos. 2011CB921800 and 2013CB921700) and the National Natural Science Foundation of China (No. 11374339).

[1]I. G. Baek, D. C. Kim, M. J. Lee, H.-J. Kim, E. K. Yim, M. S. Lee, J. E. Lee, S. E. Ahn, S. Seo, J. H. Lee, J. C. Park, Y. K. Cha, S. O. Park, H. S. Kim, I. K. Yoo, U.-I. Chung, J. T. Moon, and B. I. Ryu, IEDM Tech. Dig. **2005**, 750.
[2]R. Waser and M. Aono, Nat. Mater. **6**, 833 (2007).
[3]H. Akinaga and H. Shima, Proc. IEEE **98**, 2237 (2010).
[4]S. Seo, M. J. Lee, D. H. Seo, E. J. Jeoung, D.-S. Suh, Y. S. Joung, I. K. Yoo, I. R. Hwang, S. H. Kim, I. S. Byun, J.-S. Kim, J. S. Choi, and B. H. Park, Appl. Phys. Lett. **85**, 5655 (2004).
[5]S. B. Lee, S. C. Chae, S. H. Chang, J. S. Lee, S. Seo, B. Kahng, and T. W. Noh, Appl. Phys. Lett. **93**, 212105 (2008).
[6]B. J. Choi, D. S. Jeong, S. K. Kim, C. Rohde, S. Choi, J. H. Oh, H. J. Kim, C. S. Hwang, K. Szot, R. Waser, B. Reichenberg, and S. Tiedke, J. Appl. Phys. **98**, 033715 (2005).
[7]C. Hu, M. D. McDaniel, J. G. Ekerdt, and E. T. Yu, IEEE Electron Device Lett. **34**, 1385 (2013).
[8]S. Kim, H. Moon, D. Gupta, S. Yoo, and Y.-K. Choi, IEEE Trans. Electron Devices **56**, 696 (2009).
[9]Y.-D. Chiang, W.-Y. Chang, C.-Y. Ho, C.-Y. Chen, C.-H. Ho, S.-J. Lin, T.-B. Wu, and J.-H. He, IEEE Trans. Electron Devices **58**, 1735 (2011).
[10]I. G. Baek, M. S. Lee, S. Seo, M. J. Lee, D. H. Seo, D.-S. Suh, J. C. Park, S. O. Park, H. S. Kim, I. K. Yoo, U.-I. Chung, and J. T. Moon, IEDM Tech. Dig. **2004**, 587.
[11]B. Gao, H. W. Zhang, S. Yu, B. Sun, L. F. Liu, X. Y. Liu, Y. Wang, R. Q. Han, J. F. Kang, B. Yu, and Y. Y. Wang, IEEE Electron Device Lett. **30**, 1326 (2009).
[12]F. Miao, J. P. Strachan, J. J. Yang, M.-X. Zhang, I. Goldfarb, A. C. Torrezan, P. Eschbach, R. D. Kelley, G. Medeiros-Ribeiro, and R. S. Williams, Adv. Mater. **23**, 5633 (2001).
[13]M. Terai, Y. Sakotsubo, S. Kotsuji, and H. Hada, IEEE Electron Device Lett. **31**, 204 (2010).
[14]X. Wu, P. Zhou, J. Li, L. Y. Chen, H. B. Lv, Y. Y. Lin, and T. A. Tang, Appl. Phys. Lett. **90**, 183507 (2007).
[15]H. Zhang, B. Gao, B. Sun, G. Chen, L. Zeng, L. Liu, X. Liu, J. Lu, R. Han, J. Kang, and B. Yu, Appl. Phys. Lett. **96**, 123502 (2010).
[16]Y. C. Yang, F. Pan, Q. Liu, M. Liuand, and F. Zeng, Nano Lett. **9**, 1636 (2009).
[17]R. Waser, R. Dittmann, G. Staikov, and K. Szot, Adv. Mater. **21**, 2632 (2009).
[18]R. Dong, W. F. Xiang, D. S. Lee, S. J. Oh, D. J. Seong, S. H. Heo, H. J. Choi, M. J. Kwon, M. Chang, M. Jo, M. Hasan, and H. Hwang, Appl. Phys. Lett. **90**, 182118 (2007).
[19]C. Y. Lin, C. Y. Wu, C. Y. Wu, T. C. Lee, F. L. Yang, C. Hu, and T. Y. Tseng, IEEE Electron Device Lett. **28**, 366 (2007).
[20]W. Guan, S. B. Long, R. Jia, and M. Liu, Appl. Phys. Lett. **91**, 062111 (2007).
[21]W. Y. Chang, K. J. Cheng, J. M. Tsai, H. J. Chen, F. Chen, M. J. Tsai, and T. B. Wu, Appl. Phys. Lett. **95**, 042104 (2009).
[22]Q. Liu, S. Long, H. Lv, W. Wang, J. Niu, Z. Huo, J. Chen, and M. Liu, ACS Nano **4**, 6162 (2010).
[23]I. Turyan, U. O. Krasovec, B. Orel, T. Saraidorov, R. Reisfeld, and D. Mandler, Adv. Mater. **12**, 330 (2000).
[24]C. Bechinger, G. Oefinger, S. Herminghaus, and P. Leiderer, J. Appl. Phys. **74**, 4527 (1993).
[25]B. Ingham, S. C. Hendy, S. V. Chong, and J. L. Tallon, Phys. Rev. B **72**, 075109 (2005).
[26]M. G. Cao, Y. S. Chen, J. R. Sun, D. S. Shang, L. F. Liu, J. F. Kang, and B. G. Shen, Appl. Phys. Lett. **101**, 203502 (2012).
[27]D. S. Hong, Y. S. Chen, Ying Li, H. W. Yang, L. L. Wei, B. G. Shen, and J. R. Sun, Sci. Rep. **4**, 4058 (2014).
[28]M. Gillet, C. Lemire, E. Gullet, and K. Aguir, Surf. Sci. **532–535**, 519 (2003).
[29]S. Zafar, R. E. Jones, B. Jiang, B. White, P. Chu, D. Taylor, and S. Gillespie, Appl. Phys. Lett. **73**, 175 (1998).